The final publication is available at

https://doi.org/10.1109/JSEN.2020.3042653

A fast method for monitoring the shifts in resonance frequency and dissipation of the QCM sensors of a Monolithic array in biosensing applications

Román Fernández[1,2], María Calero[1], José Vicente García[2], Ilya Reviakine[2,3], Antonio Arnau[1] and Yolanda Jiménez[1]

[1] Centro de Investigación e Innovación en Bioingeniería, Universitat Politècnica de València, 46022 Valencia, Spain
[2] Advanced Wave Sensors S.L. 46988, Paterna, Valencia, Spain
[3] Department of Bioengineering, University of Washington, Seattle, WA, 98150, USA

Abstract—— Improvement of data acquisition rate remains as an important challenge in applications with Quartz Crystal Microbalance (QCM) technology where high throughput is required. To
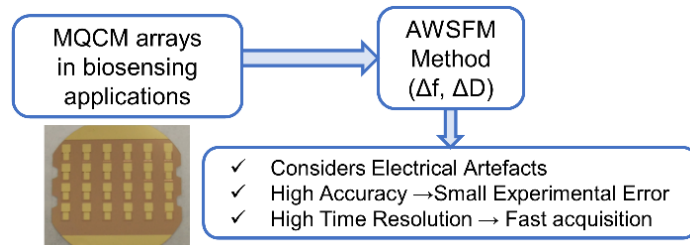
address this challenge, we developed a fast method capable of measuring the response of a large number of sensors and/or overtones, with a high time resolution. Our method, which can be implemented in a low-cost readout electronic circuit, is based on the estimation of Δf_r (frequency shift) and ΔD (dissipation shift) from measurements of the sensor response obtained at a single driving frequency. By replacing slow fitting procedures with a direct calculation, the time resolution is only limited by the physical characteristics of the sensor (resonance frequency and quality factor), but not by the method itself. Capabilities of the method are demonstrated by monitoring multiple overtones with a single 5 MHz sensor and a Monolithic QCM array comprising 24 50MHz-sensors. Accuracy of the method is validated and compared with the state-of-the-art, as well as with a reference method based on impedance analysis.

Index Terms— Biosensor, Fast acquisition, Monolithic Quartz Crystal Microbalance (MQCM), Multiple overtones, Sensor array devices.

I.   Introduction

Analytical techniques based on Quartz Crystal Microbalance (QCM) have been steadily growing mainly driven by advantageous features such as: 1) direct label-free detection; 2) real-time non-invasive approach; 3) low cost and 4) ability to detect mass, viscoelastic and conformational changes occurring on the sensor surface. Point-of-care diagnosis [1], [2], security, environmental and food safety monitoring [3], are key application fields for QCM technology. In these fields, novel technical developments such as the use of highly sensitive sensor designs for multi-analyte detection and the improvement of the physical interpretation of the different phenomena occurring on the sensor surface will contribute

to strengthen QCM technology [4], [5]. Recently, a highly sensitive QCM immunosensor has been successfully developed and tested for its use in pesticide determinations in food. An improvement of two orders of magnitude in Limit of Detection (LOD), when comparing with that reported for traditional 9 MHz QCM, has been achieved by combining a low-noise interface readout circuit with 100 MHz High Fundamental Frequency (HFF) QCM sensors [6]–[9]. The increment in the frequency, originated from the reduction of the sensor thickness [10], provides more sensitive resonators with a reduced surface area [11]. Size reduction allows for their integration in an array configuration, giving rise to the Monolithic QCM (MQCM) technology [12]–[20]. MQCM offers a unique approach to miniaturizing and parallelizing QCM-based assays, thus improving the throughput and reducing reagent consumption. MQCM places stringent requirements on the readout circuit. Most importantly, a high acquisition rate is required for rapidly characterizing all of the array elements. This is particularly important when probing the resonators at multiple overtones. Multiple overtone measurements are increasingly recognized as an important extension of the QCM technique. They are needed for enhancing physical interpretation of the different phenomena occurring on the sensor surface [21].

In a typical QCM experiment, the magnitudes acquired are the shifts in the resonance frequency, Δf_r, and the dissipation, ΔD (equivalent to the half-bandwidth $\Delta\Gamma$), at one or more overtones. These relevant electric parameters of the resonant sensors are related with the physical and/or biochemical properties of the layers deposited over them through various models. These models can be found in references [22], [23]. In other words, a high resolution and fast operation readout system that provides Δf_r and ΔD is required to match the capabilities of MQCM and drive the development of QCM technology. While the classical impedance spectrometry has been routinely used for sensor characterization, mainly in very high frequency applications, the readout systems based on this method are costly and not fast enough to access many sensors in MQCM arrays, because it is difficult to lower the time per sweep below 0.5 s [24]. The time limitations of the impedance spectrometry method become even more severe when the measurements need to be done on multiple overtones [25]. Ring-down methods also provide measurements at multiple overtones, but their operation frequency is limited up to 70 MHz, thus limiting the sensibility [10], [26], [27]. Moreover, they require a high processing time (~ 1s per overtone [24]), thus preventing its use for a fast tracking of the processes occurring on multiple resonators in MQCM technology. Oscillators are faster than the previously mentioned systems. Their main drawbacks have been pointed out when working in-liquid applications and with high frequency resonators [28]–[32].

Arnau and coworkers [32], [33] proposed an alternative readout circuit based on the tracking of the sensor phase at a fixed excitation frequency. This characterization circuit can work with HFF-QCM sensors with limited phase and frequency noises, thus improving the LOD [31]. The approach allows for a low-cost implementation of the electronics and high integration capability, which, together with its high operation speed, opens the possibility of combining sequential acquisition with multichannel parallel detection in MQCM, even when probing them on multiple overtones. The circuit directly measures the phase and amplitude response of the resonator at a fixed frequency. A direct relationship between the measured phase shift and the mass variation of the layer over the resonator is provided. This relationship is only valid when, along the experiment, the

resonator works in gravimetric regime (variations on the resonator amplitude are negligible) and the frequency changes are extremely small. Moreover, neither Δfr nor ΔD are provided. These aspects limit the applicability of the approach proposed in references [32], [33] for bioanalytical applications. Recently, other authors [34], [35] have proposed a method based on the measurement of the sensor impedance at a single fixed driving frequency that assumes that the sensor characteristic impedance zq remains invariant during the experiment. The method, named Fixed Frequency Drive (FFD), provides Δfr and ΔD, but it does not take into account the electrical parasitic effects. The non-consideration of these parasitic effects could lead to errors in the sensor characterization.

This paper introduces a single-frequency-based QCM characterization method named Acoustic Wave Single Frequency Measurement (AWSFM) for measuring Δfr and ΔD at multiple overtones. The method uses the hardware introduced by Arnau and co-workers in references [32], [33] with a new approach to provide Δfr and ΔD. AWSFM fast method considers, not only the motional properties of the resonator (directly related to the biochemical and physical properties of the layers), but also the electrical parasitic effects [24]. Impedance spectrometry analysis accounts for these parasitic effects through the fitting of resonance models to entire frequency sweeps. This makes the measurement more robust against the electrical artefacts at the cost of slowing down the operation speed. Instead, AWSFM method performs an initial fitting of the sensor admittance spectrum, followed by a calculation of the frequency and dissipation shifts from a measurement at a single testing frequency. Therefore, our method combines the speed of a readout interface circuit working at a single frequency with the advantages of impedance analysis that allows electrical parasitic effects to be taken into account.

Two different versions of AWSFM method are presented in this work. The only meaningful difference between the two implementations is the testing frequency selection procedure. While AWSFM-Fixed Frequency (AWSFM-FF) keeps the sensor testing frequency fixed during the whole experiment (represented in Figure 1 in green color), AWSFM-Tracking (AWSFM-T) updates the testing frequency continuously by adjusting its value to the current sensor resonance frequency (represented in Figure 1 in blue color).

To evaluate the performance and accuracy of AWSFM method, we first carry out a parametric study based on the offline post-processing of real experimental data, which lets us test the influence of the different parameters affecting the method accuracy separately. Then, both versions are implemented and tested in real-time experiments for two significant applications: characterization of 1) multiple overtones in an individual sensor for two different experiments: water to water-glycerol mixture medium exchange and electrochemical deposition of copper; and 2) multiple sensors integrated in a Monolithic QCM array for direct adsorption of Neutravidin.
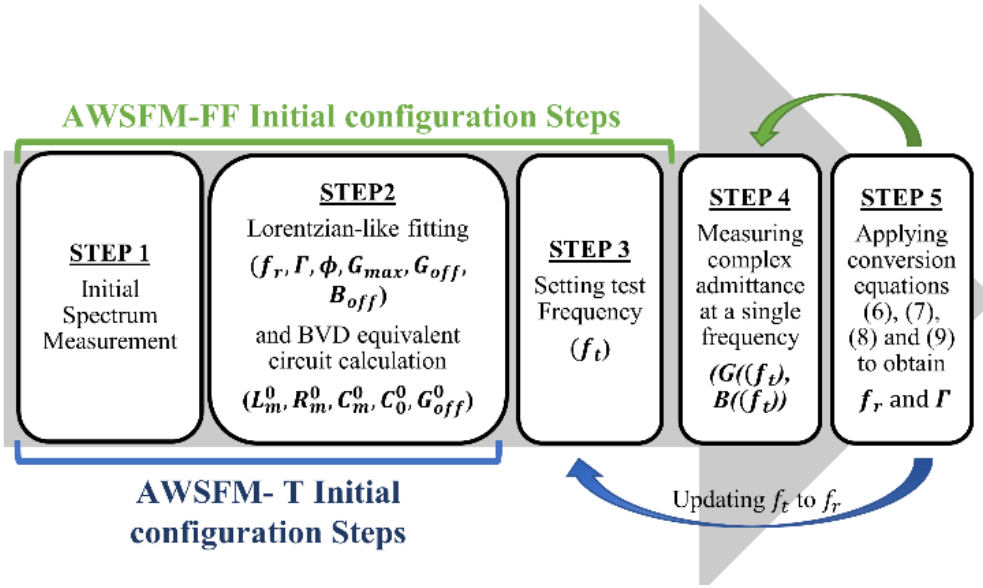
Fig. 1. Flow diagrams describing the different steps of both approaches AWSFM-FF (Green) and AWSFM-T (blue) to estimate the values of f_r and D (or Γ).

II.   Materials and Methods

A.   Description of the novel characterization method

Our QCM characterization method is based on the application of the well-known Butterworth-van-Dyke (BVD) model. The BVD equivalent circuit models the response of the uncoated QCM sensor close to its resonance frequencies [36]. The model has two branches: the first one is known as "static branch" that is formed by a capacitor C0, which is associated with the electrical capacitance of the dielectric material of the quartz resonator. The second branch is the so-called "motional branch" and it is formed by an LCR series circuit (Rm, Lm and Cm). A third branch containing a frequency dependent conductance (Goff) can be added to consider the experimental increment of the conductance baseline with the frequency [24], [37], [38]. Each one of the electrical elements of the motional branch is related to the mechanical properties of the resonator.

The AWSFM method yields the changes in the resonance frequency and in the dissipation of the sensor (Δfr and ΔD) from the real and imaginary parts of the electrical sensor admittance measured at a single testing frequency. Next, the equations that define AWSFM are introduced. (It is important to mention that the applicability of the method requires an initial estimation of the whole set of the BVD circuit parameters -R_m^0, L_m^0, C_m^0, Goff and C_0^0-, and to assume that no changes will occur in Cm and C0 during the experiment).

The complex admittance of the sensor predicted by the BVD equivalent circuit is:

$$Y_X = G(\omega_t) + jB(\omega_t) = [R_m/(R_m^2 + X_m^2)] + j\omega_t C_0 - j[X_m/(R_m^2 + X_m^2)] \quad (1)$$

where ωt is the angular frequency at which the admittance is measured (ωt=2πft where ft is the testing frequency), G is the conductance after subtracting G_{off} value, B is the susceptance, and Xm is defined as:

$$X_m = L_m\omega_t - [1/(C_m\omega_t)] \quad (2)$$

Separating real and imaginary parts in (1) and rearranging the terms, Equations (3) and (4) are obtained:

$$G(\omega_t) = 1/[R_m(1 + (X_m^2/R_m^2))] \quad (3)$$

$$B(\omega_t) = \omega_t C_0 - \left[(X_m/R_m)/\left[R_m\left(1 + (X_m^2/R_m^2)\right)\right]\right] \quad (4)$$

Operating with (3) and (4), it is possible to obtain the relation (5):

$$(X_m/R_m) = \left(\omega_t C_0 - B(\omega_t)\right)/G(\omega_t) \quad (5)$$

Substitution of (5) into (3) leads to Equation (6) that allows the changes in the resistance associated to the losses in the sensor from the measurement of the admittance at the angular frequency ωt to be estimated:

$$R_m = 1/\left[G(\omega_t)\left[1 + \left(\omega_t C_0 - B(\omega_t)\right)^2/G(\omega_t)^2\right]\right] \quad (6)$$

Combining Equations (2) and (5) and solving for Lm, Equation (7) is obtained.

$$L_m = (R_m/\omega_t)\left[\left(\omega_t C_0 - B(\omega_t)\right)/G(\omega_t)\right] + 1/(\omega_t^2 C_m) \quad (7)$$

Finally, the motional series resonant frequency fr can be calculated directly from the well-known Equation (8). Lm is obtained from Equation (7), and Cm=C_m^0 is calculated in the initial fitting of the admittance spectrum of the sensor and kept constant.

$$f_r = 1/\left(2\pi\sqrt{L_m C_m}\right) \quad (8)$$

The dissipation factor D and the half-bandwidth Γ are then obtained from Lm and Rm values by applying the BVD relation for the quality factor [36]:

$$D = 1/Q = 2\Gamma/f_r = R_m/(2\pi f_r L_m) \quad (9)$$

Equations (6) and (8) can be applied to estimate, respectively, the value of the resistance and the resonance frequency of a QCM sensor in real time from the complex admittance of the sensor monitored at a single frequency. Equation (9) can be alternatively used instead of Equation (6) to estimate losses in the sensor through the dissipation or the half-bandwidth parameters. It is worthwhile mentioning that changes in Cm and C0 lead to errors in Δfr or ΔD estimated with the method; we discuss this in the section III.

Practical implementation of AWSFM method is described next. Most of the steps are identical in AWSM-FF and AWSM-T approaches; the only meaningful difference lies on whether the testing frequency is updated or not (see Figure 1):

STEP 1: Electrical artefacts affecting the sensor response are considered by performing an initial sweep of the complex electrical admittance spectrum in the 3dB bandwidth around the resonance.

STEP 2: Nelder-Mead Simplex algorithm [39] is used to fit the measured spectrum (G(f) and B(f)) to a "phase-shifted-Lorentzian" function described in [24].

$$G(f) = G_{max}\left(\frac{f^2(2\Gamma)^2}{(f_r^2 - f^2)^2 + f^2(2\Gamma)^2}\cos\phi - \frac{f(2\Gamma)(f_r^2 - f^2)}{(f_r^2 - f^2)^2 + f^2(2\Gamma)^2}\sin\phi\right) + G_{off} \quad (10)$$

$$B(f) = G_{max}\left(\frac{f^2(2\Gamma)^2}{(f_r^2 - f^2)^2 + f^2(2\Gamma)^2}\sin\phi + \frac{f(2\Gamma)(f_r^2 - f^2)}{(f_r^2 - f^2)^2 + f^2(2\Gamma)^2}\cos\phi\right) + B_{off} \quad (11)$$

where fr is the resonance frequency, G_{max} is the maximum conductance, G_{off} is the conductance offset, B_{off} is the susceptance offset, Γ is resonance half-bandwidth that is directly related to dissipation and ϕ is a shift angle accounting for a slight tilt of the resonance curve in the complex plane, which is often found. From these parameters, the values of the BVD elements can be directly obtained [36]:

$$R_m^0 = 1/G_{max} \qquad (12)$$
$$L_m^0 = R_m/(4\pi\Gamma) \qquad (13)$$
$$C_m^0 = 1/(4\pi^2 f_r^2 L_m) \qquad (14)$$
$$C_0^0 = B_{off}/2\pi f_r \qquad (15)$$

This procedure results in the values of the parameters G_{off}^0, R_m^0, L_m^0, C_m^0, and C_0^0 that best represent the initial response of the sensor.

STEP3: The testing frequency, ft, is set to the value of fr obtained in step 2. This step is just called once in AWSFM-FF implementation of the method, while it is called continuously in AWSFM-T implementation to keep the testing frequency updated to the fr value throughout the experiment.

STEP 4: Values of G and B are monitored at the testing frequency ft during the experiment (G(ωt) and B(ωt)).

STEP 5: Equations (6), (7), (8) and (9) are used to calculate the values of fr and losses (Rm, D or Γ) from G(ωt) and B(ωt) measured in step 4 and from the initial values of Cm and C0 extracted in step 2 (C_m^0 and C_0^0). The resonance frequency fr obtained in this step is used to update the testing frequency in step 3 of AWSFM-T method.

B.   Instrument and devices

1.   Sensors

Individual, circular, 14 mm 5 MHz QCM sensors (AWSensors S.L., Valencia, Spain), that were used in this study, are AT-cut bevelled plano-plano quartz crystals coated with circular wrapped gold electrodes. MQCM arrays (AWSensors S.L.) comprised 24 HFF-QCM sensors integrated in a 1-inch circular AT-cut quartz wafer. The fundamental frequency of the resonators in these arrays is 50 MHz, and their surfaces are flat and polished. The working side of the array is a grounded common electrode to avoid capacitive coupling through the liquid (see Section SI in the supporting information).

To clean the sensors, they were exposed to UV radiation for 10 min in a UV/ozone cleaner (BioForce Nanosciences Inc., Chicago, IL, USA), rinsed with 99% pure ethanol, rinsed with bi-distilled water, dried with ultra-pure nitrogen gas (Al Air Liquide España, S.A.) using a gas filter pistol equipped with a 1 μm pore diameter PTFE filter (Skan AG, Allschwil, Switzerland), and treated again with UV/ozone for 10 min.

2.   Sensor electrical characterization

AWS X1 platform (AWSensors S.L.) was used to characterize individual 5 MHz sensor response. This Quartz Crystal Microbalance with Dissipation (QCMD) instrument is based on the fixed-frequency phase-shift measurement technique described elsewhere [33]. AWS X1 incorporates several operation modes including a characterization method based on classical impedance spectroscopy that provides both frequency and dissipation information. This operation mode was used as a reference method in this work. AWS X24 platform (AWSensors S.L.) was used to characterize MQCM array response. This device is based on the same core technology as AWS X1 system and is capable of measuring simultaneously the acoustic response of up to 24 HFF-QCMD sensors. AWSuite software package (AWSensors S.L.) has been used to control both instruments and to register and process the acquired data.

C.   Experimental

1.   Water to water-glycerol mixture medium exchange measurement protocol

Double distilled water-Glycerol mixtures (25%) were prepared. Their theoretical viscosities and densities are 1.386 Pa·s and 1061.15 kg/m3, respectively [40]. 5 MHz QCM sensors were mounted into a measurement flow-cell (AWSensors S.L.). AWS Flow Control Unit, (AWSensors S.L.) was used to generate a uniform flow through the sensor

cell. A flow rate of 50μl/min was set. Temperature, controlled with the integrated Peltier elements, was set to 23°C. Assay procedure was as follows: 1) Sensor stabilization under flow of bi-distilled water until stable baselines for frequency and dissipation are achieved. 2) Glycerol injection for 12.5 min. 3) Bi-distilled water flow through the sensor. Steps 2) and 3) are repeated 3 times.

2.   *Electrochemical deposition of copper*

Copper sulphate (CuS04) dissolution 10 mM was prepared using double distilled water. Electrochemical quartz crystal microbalance experiments were carried out with a SP-200 potentiostat/galvanostat (Biologic, Grenoble, France). A cyclic voltammetry was carried out using a conventional three-electrode in-batch cell (AWSensors S.L.). Top surface of a 5 MHz QCM sensor was used as the working electrode. The reference electrode was Ag|AgCl with a 3 M NaCl internal solution (RE-1B, ALS Co., Ltd, Tokyo, Japan) and the counter electrode was a platinum partially coiled wire (ALS Co., Ltd). Cyclic voltammograms were registered at a sweep rate of 20 mV s−1. Maximum and minimum vertex potentials were set to 0.5 V and -0.22 V, respectively. Three cycles were measured with each method to check the repeatability of the experiment.

3.   *Neutravidin adsorption over MQCM array*

Neutravidin adsorption was measured using three different characterization methods: reference impedance spectrometry method, AWSFM-T and AWSFM-FF. 8 sensors of the same array were monitored in each experiment. A MQCM custom flow measurement cell (Jobst Technologies, Freiburg, Germany) was used. Fluidic channels were filled with PBS at a flow rate of 20 μL/min. Baseline signals were acquired for ~ 5 – 10 min, followed by the injection of neutravidin (at a concentration of 100 μg/mL in PBS). See Supplementary information SI for further details.

D.   Chemicals

Nanopure water used in this study was either analytical grade water (Panreac Química SLU, Barcelona, Spain), or produced with a Smart2Pure UVUF water purification system (Thermo Fisher Scientific, Barcelona, Spain). Pure ethanol was purchased from Panreac Química SLU (Barcelona, Spain) and Glycerol was purchased from Scharlab (Barcelona, Spain) with 99.5% reagent grade. Phosphate buffered saline (PBS) tablets for preparing 0.01 M phosphate buffer containing 0.0027 M potassium chloride and 0.137 M sodium chloride, pH 7.4, at 25 °C were purchased from Sigma Aldrich Química, S.L.U. (Madrid, Spain). NeutrAvidin and Sodium Dodecyl Sulfate (SDS) 20% solution were purchased from Fisher Scientific S.L. (Madrid, Spain). COBAS Cleaner was purchased from Sanilabo S.L. (Valencia, Spain).

III.   Results and Discussion

A.   Parametric Study of the characterization methods

A parametric study based on the offline processing of real QCMD experiments was performed to deepen our understanding of the AWSFM method. In this study, we developed a custom software code to simulate the admittance spectrum of the sensor at any driving frequency starting from the six parameters of the "phase-shifted-Lorentzian" model described in Eq. 10 and 11. These parameters (fr, G_{max}, G_{off}, B_{off}, Γ and ϕ) were gathered from real experiments monitored along the time by using classical impedance spectrometry. We have used real data as starting point, instead of ideal ones, in order to obtain a more accurate evaluation of the method. Our software code also implements AWSFM method to calculate the expected resonance frequency and dissipation shifts from the simulated admittance spectrum (See Supplementary information SII for further details). We have also included FFD method proposed by Guha and co-workers [34] in

our analysis for comparison. Two representative cases were chosen to test the proposed method: 1) a rigid layer contacting a Newtonian medium and 2) a semi-infinite Newtonian medium exchange.

In the first case, AWSFM-FF and AWSFM-T results agree well with the experimental frequency data (see Figure 2(a)). FFD method underestimates the frequency shift for $|\Delta fr|$ values higher than 500 Hz. However, it behaves well for small frequency shifts. We attribute the limited operating range of FFD method to the assumption that the sensor characteristic impedance ($z_q = \sqrt{L_m/C_m}$), i.e., Lm to Cm ratio, does not change during the experiment. Unlike the FFD method, AWSFM-FF and AWSFM-T methods consider Lm variations (Cm is kept constant throughout the experiment). From our point of view, the latter assumption fits better with the nature of QCM experiments, where mass transfer processes at the sensor surface are studied, since theoretical physical meaning of Lm parameter is indeed directly related to mass changes [36].

AWSFM-T is the only scheme that provides an accurate estimation of the half-bandwidth shift (see Figure 2(b)). Methods based on the fixed testing frequency that is not updated during the experiment (AWSFM-FF and FFD) fail to reproduce the experimentally observed changes in the half-bandwidth when the $|\Delta fr|$ is greater than 500Hz.
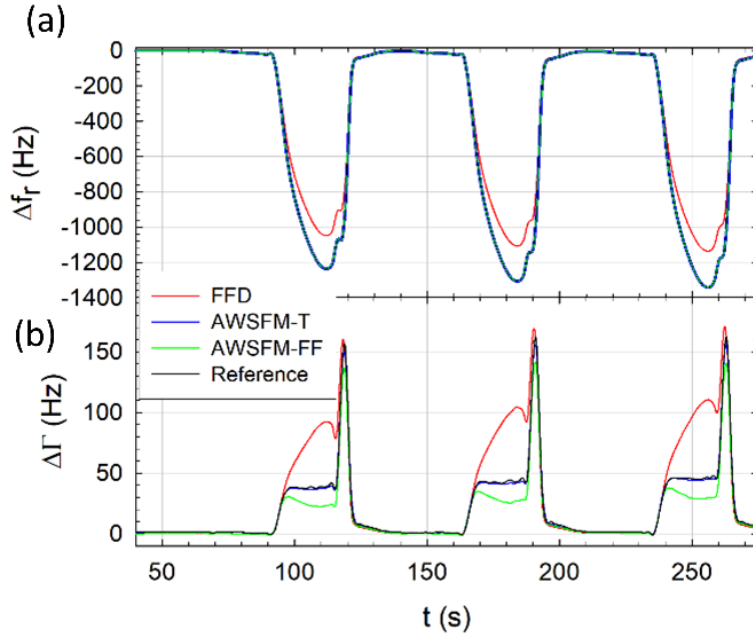

Fig. 2. Resonance frequency (a) and half-bandwidth (b) shifts versus time for a rigid layer contacting a Newtonian medium obtained experimentally (black) and with the simulated methods: AWSFM-T (blue), AWSFM-FF (green) and FFD (red).

Simulation was extended to all the overtones acquired (from 1st to 13th) for the two representative experimental conditions. A general trend that was observed for all three methods is that the errors are considerably larger in half-bandwidth dissipation than in the frequency determination. This is shown in Figure 3, where it can be seen that the errors in the half-bandwidth are especially significant in the case of a rigid layer contacting a Newtonian medium for the fixed-frequency methods (AWSFM-FF and FFD). Furthermore, the errors in the case of the FFD method are always larger than in the case of the other two methods, both for the frequency, and for the half-bandwidth. On the other hand, the AWSFM-FF achieves a good accuracy in fr, but exhibit higher errors in Γ than the AWSFM-T method, which is the most accurate of all three for both fr and Γ. AWSFM-T errors do not exceed 2.02 ppm for fr and 4482 ppm for Γ for both

experimental conditions.

Since the methods are based on the estimation of sensor admittance at a single testing frequency while assuming constant C0 and Cm parameters, we hypothesize that validity ranges and accuracies of fixed frequency methods could be affected by the nature of the changes in the admittance spectrum "shape". If fr variations are larger than Γ, then fr starts to move away from ft. When the gap between fr and ft becomes of the same order of magnitude as the sensor resonance 3 dB span, error increases in those fixed frequency methods. A detailed discussion about this point can be found in SIII of Supplementary Information.

After comparing the accuracy of the methods, we studied their sensitivity to the initial value selection of ft and C0. Since AWSFM-T is directly based on the continuous update of the testing frequency, we just studied the influence of ft selection for AWSFM-FF and FFD methods. Although the influence of this parameter is not very significant in fr measurements, which is in agreement with other author results [34], our calculations show a strong dependence in the determination of Γ on the testing frequency for both methods. This behavior is consistent for the two experimental conditions considered (see Supplementary Information SIV for further details).
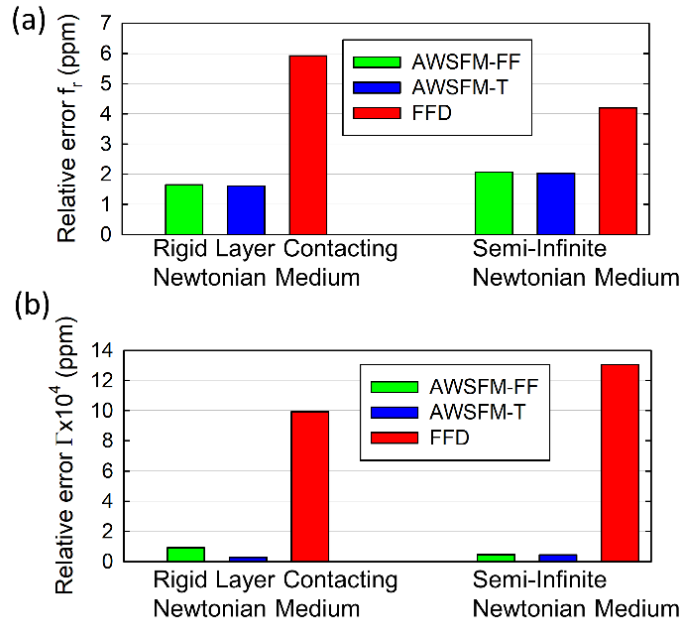

Fig. 3. Simulated resonance frequency (a) and half-bandwidth (b) absolute relative error (in parts per million) with respect to experimental data for a semi-infinite Newtonian medium exchange and a rigid layer contacting a Newtonian medium for AWSFM-T (blue bar), AWSFM-FF (green bar) and FFD method (red bar).

We also considered the influence of the initial value of C0 on the results obtained with the different methods. Since this parameter is especially sensitive to the parasitic capacitances produced by wires, connectors, and electrical contacts in the measurement cells, it is normally responsible of most of the electrical artefacts affecting the sensor response. A calculation of the influence of a small variation in C0 on the accuracy for the three characterization methods reveals that the error is not negligible in the determination of the half bandwidth (see further details in Supplementary Information SV).

B.   Real time measurements in multiple overtone experiments

To show the capabilities of AWSFM method in real applications, AWSFM-T and

AWSFM-FF were implemented in the AWS X1 platform by developing a custom firmware code. Two experiments were monitored in real time: a water to water-glycerol (25%) mixture and a copper electrodeposition over the sensor top electrode surface.

The results of the measurements performed with the water-glycerol mixtures are shown in Figure 4. It can be seen that Δf_r and $\Delta \Gamma$ measurements obtained with both methods exhibit a good linearity with respect the square root of the overtone order n predicted by the Kanazawa-Gordon-Mason equation [41], with R-squared larger than 0.993. AWSFM-FF average relative error is 7.04% for Δf_r and 2.76% for $\Delta \Gamma$. AWSFM-T average relative error is 5% for Δf_r and 1.7% for $\Delta \Gamma$. An explanation for why the errors are close in this case is provided in the SIII of the supplementary information.
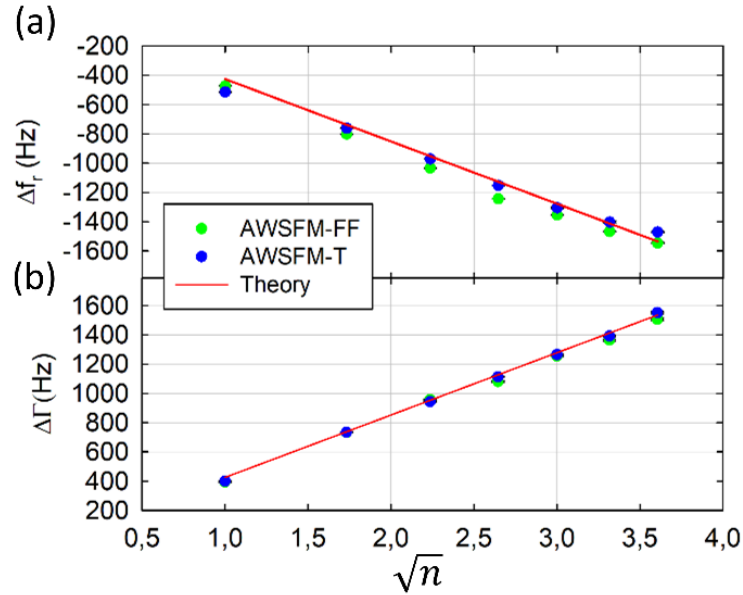

Fig. 4. Shifts in frequency (a) and half-bandwidth (b) registered after the injection of water-glycerol mixture (25% in concentration). Both, AWSFM-FF (green circles) and AWSFM-T (blue circles) methods are depicted with the theoretical value predicted by Kanazawa-Gordon-Mason equation (red line).

Figure 5 shows the results of the copper electrodeposition experiments. AWSFM-T results, both for Δf_r /n and $\Delta \Gamma$/n, are in good agreement with the reference method (impedance analysis). Larger errors are observed with the AWSFM-FF method than with the AWSFM-T method, which concurs with the simulation results presented above. AWSFM-FF method underestimates Δf_r /n values at higher frequencies (with the increasing overtone order n), while the measured $\Delta \Gamma$/n values are underestimated or overestimated for different n. Considering all overtones in the calculation, the average relative error in Δf_r /n is 7.11% and 151.38% in $\Delta \Gamma$/n for the AWSFM-FF method, and 0.89% and 2.73% for the AWSFM-T method.

C.   Real time measurements in Neutravidin direct adsorption over a MQCM device

Finally, direct adsorption of neutravidin (NAV) over the gold surface was monitored using a MQCM device comprising 24 HFF-QCM sensors operating at a fundamental frequency of 50 MHz. Average crosstalk between neighbor sensors was measured to be around -65 dB. This value assures the independence of the sensor response and it is better than -50 dB, recently reported for 150 MHz HFF-QCM arrays [42]. Neutravidin is commonly used in biosensing applications to prepare the sensor surface for further chemical modification [43]–[47].
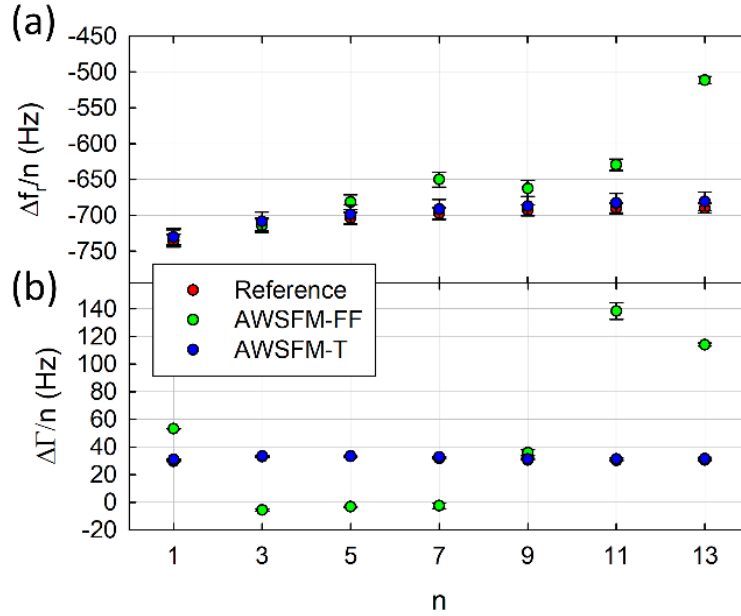
Fig. 5. Normalized shifts in resonance frequency (a) and half-bandwidth (b) versus overtone order. Values were taken at the value of minimum frequency shift of the voltammetry cycle for 3 consecutive cycles. AWSFM-FF (green circles) and AWSFM-T (blue circles) methods are compared with the reference impedance spectroscopic method (red circles). Error bars are included in the graphs to show the measurement variance.

Figure 6 shows the average resonance frequency and dissipation shifts measured over the 8 sensors tested by each method. ΔD is used in this section instead of $\Delta\Gamma$ for easier comparison with the literature. Impedance analysis, which is used here as a reference, provides an average Δf_r value of -6075 ± 155 Hz. Considering a Sauerbrey coefficient of -0.1765 ng· cm-2 Hz-1 for 50 MHz sensors, an average areal mass density of 1072 ± 27 ng·cm-2 can be estimated. This value is in good agreement with the literature. Wolny et al. reported a mass density of 1081 ng·cm-2, working with 4.95 MHz sensors [45]. Hays et al. reported 920 ng·cm-2 at 5 MHz as a first step to build a gold QCM haemoglobin immunosensors [46]. Boujday et al. reported 980 ng·cm-2 working at 3rd overtone of a 5MHz QCM to study the adsorption on Neutravidin and its relation to the efficiency of biosensors [47]. Tsortos and coworkers have reported mass densities from 908 to 1261 ng·cm-2 at the seventh overtone of a 5 MHz QCM in their works using Neutravidin to study DNA conformation [43], [44].

The absolute value of the dissipation is somewhat more difficult to discuss: it is frequency-dependent, because the rate at which energy is dissipated at the oscillating solid/liquid interface depends on the frequency. This limits the ability to compare our results, obtained with the 50 MHz sensors, with the literature, where low frequency sensors are normally used. A useful qualitative argument can, however, be made. A near-zero dissipation shift is expected for a Sauerbrey-like protein layer, but Neutravidin adsorption typically results in non-Sauerbrey behaviour. Therefore, we take our impedance analysis results at face value, as they are consistent with the literature in this qualitative sense. The important consideration for the purposes of this work is whether the AWSFM-T and -FF methods accurately reproduce the results of the impedance analysis.

For future reference, we quote a value of $0.0045 \cdot 10$-6/Hz for the so-called acoustic ratio, $\Delta D/\Delta f_r$. Acoustic ratio is a parameter that depends on molecular geometry and the geometry of binding of the molecule to the surface [48], but not on other details of the experiment. It is also frequency-dependent. We note that our observed value is close to that reported by Tsortos and co-workers ($0.0046 \cdot 10$-6/Hz at 35 MHz, the seventh

overtone of a 5 MHz sensor) [43]. Both these values are smaller than that of Wolny et al. (0.03·10-6/Hz at 4.95 MHz) [45], or Boujday et al. (0.018·10-6/Hz at 15 MHz) [47], confirming the expected trend that acoustic ratio should decrease with the resonance frequency.

Comparing the ability of the AWSFM approaches to reproduce the results of the impedance analysis (Figure 6), we can see that both AWSFM-FF and AWSFM-T agree well with reference method in Δfr measurements. AWSFM-FF provides a frequency shift of -6115 ± 373 Hz while AWSFM-T gives -6069 ± 181 Hz. Dissipation results provided by AWSFM-T are also in very good agreement with the reference method, but this is not the case for the AWSFM-FF method: the average ΔD measured with the AWSFM-T method is 26.4 ± 2.9·10-6, compared to the reference value of 27.3 ± 3.2·10-6. However, as it was expected from the preliminary parametric study and the real time electrodeposition experiments, fixed-frequency algorithms like AWSFM-FF fail to estimate properly the losses of the sensor unless the widening in the sensor response is of the same order as the frequency shift (see a qualitative explanation in SIII of Supplementary information).

D.   Timing considerations

It is interesting to discuss the benefits of the different methods from the data acquisition rate point of view. As it has been previously mentioned, AWS X1 platform hardware was used to implement both AWSFM-T and AWSFM-FF schemes. Without loss of generality, instrument acquisition rate has been set to 10 ksps and a 10-samples direct averaging has been configured to improve the signal to noise ratio. Thus, AWSFM-FF implementation effective sampling rate is 1000 sps. On the other hand, AWSFM-T effective acquisition rate used in the measures presented in this paper is 250 sps. This rate depends on factors such as the calculation time required to compute the new testing frequency after each acquisition (400 µs in our case), the time required to modify the testing frequency in AWS X1 signal generator (hundreds of ns) and the settling time necessary to assure that steady-state has been reached in the sensor response after changing the testing frequency. Usually, the settling time is defined as a multiple of the relaxation time τ, defined as the time needed by an oscillator to adapt to changing external conditions.

$$\tau = Q/2\pi f_r \qquad (16)$$

As it can be inferred from Equation 16, τ will depend not only on the sensor frequency but on the operating conditions through Q. For instance, in the case of a 5 MHz sensor operating at 1st overtone in air $\tau = 3.9$ ms, for a 5 MHz sensor operating at 1st overtone in bi-distilled water $\tau = 180$ µs, for a 50 MHz sensor operating at 1st overtone in air $\tau = 180$ µs and for a 150 MHz HFF-QCM sensor operating at 1st overtone in air $\tau = 3.9$ µs. Our current AWSFM-T and AWSFM-FF implementations allow for settling time configuration. All multiple overtone experiments described in this paper have been carried out with a 5 ms settling time.
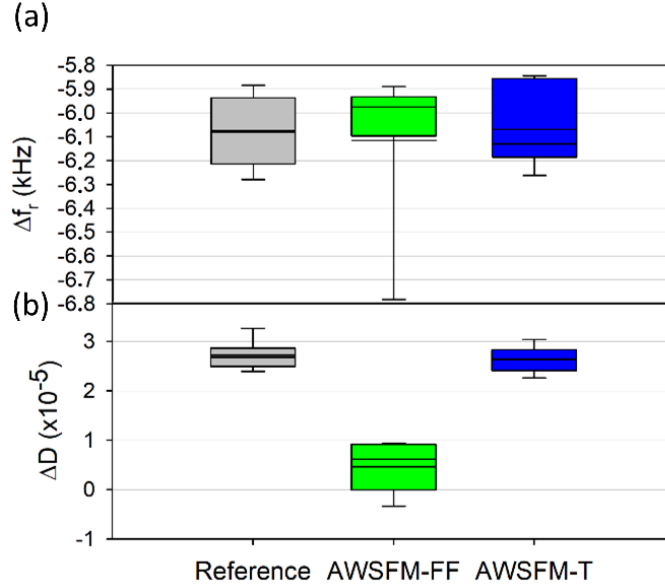
Fig. 6. (a) Average resonance frequency shift (a) and average dissipation shift (b) measured for 8 sensors of the same array using AWSFM-FF (green bar), AWSFM-T (blue bar) and reference method (grey bar) during NAV adsorption.

It is worth mentioning that it takes the reference method 12 s to characterize the 24 HFF-QCM sensors integrated in the array while AWSFM method just needs less than 300 ms. Of course, acquisition rates of the AWSFM implementations described in this paper cannot be considered as the maximum ones achievable. It is possible to modify the current instrument setup or it is even possible to use another hardware platform to obtain a higher data rate. But, leaving aside hardware considerations, the only factor that really impacts on the method throughput rate is τ. At this point, AWSFM-FF could offer an advantage over AWSFM-T since it does not require to wait for the resonance settling time because, unlike AWSFM-T, AWSFM-FF testing frequency is kept constant during the whole experiment. However, in most real applications, multiple overtone approach or sensor arrays are used. In those cases, it is necessary to change the operation frequency to characterize the next overtone/sensor in a multiplexed configuration. Thus, settling time must be respected anyway and time resolution advantages of fixed-frequency methods (AWSFM-FF and FFD) disappear. In those cases, AWSFM-T is clearly the most accurate single-frequency characterization method providing Δfr and ΔD (or ΔΓ).

IV. Conclusion

A novel characterization method (AWSFM) capable of determining the resonance frequency and dissipation through electric admittance measured at a single driving frequency has been presented in this work. Two different versions of the method have been implemented. Main difference between them lies in the selection of the testing frequency. While the first scheme, named AWSFM-FF, operates at a fixed frequency, the second scheme, named AWSFM-T, updates continuously the testing frequency tracking the resonance frequency of the resonator. A parametric study has been carried out to study the influence of the testing frequency and the parasitic capacitances on the accuracy of the method. According to our results, a bad estimation of the values of ft and C0 during the initial experiment setup could lead to a significant error increase in ΔΓ.

Both schemes have been implemented and tested in real time experiments for two representative applications. While AWSFM-FF has provided good results in Δfr, it has shown errors in ΔΓ. AWSFM-T has shown to be accurate both in Δfr and ΔΓ and it is

especially suitable for applications where a large number of sensors/overtones must be monitored simultaneously.

To the best knowledge of the authors, no other single-frequency-based characterization method has been previously used to monitor biosensing experiments simultaneously in 24 HFF-QCM sensors integrated in the same quartz substrate.

REFERENCES

[1]   M. U. Ahmed, I. Saaem, P. C. Wu, and A. S. Brown, "Personalized diagnostics and biosensors: a review of the biology and technology needed for personalized medicine," *Crit. Rev. Biotechnol.*, vol. 34, no. 2, pp. 180–196, Jun. 2014.

[2]   V. Gubala, L. F. Harris, A. J. Ricco, M. X. Tan, and D. E. Williams, "Point of Care Diagnostics: Status and Future," *Anal. Chem.*, vol. 84, no. 2, pp. 487–515, 2012.

[3]   J. L. C. M. Dorne, J. L. C. M. Dorne, L. R. Bordajandi, B. Amzal, P. Ferrari, and P. Verger, "Combining analytical techniques, exposure assessment and biological effects for risk assessment of chemicals in food," *TrAC Trends Anal. Chem.*, vol. 28, no. 6, pp. 695–707, Jun. 2009.

[4]   R. E. Speight and M. A. Cooper, "A Survey of the 2010 Quartz Crystal Microbalance Literature," *J. Mol. Recognit.*, vol. 25, no. 9, pp. 451–473, 2012.

[5]   J. P. Lafleur, A. Jönsson, S. Senkbeil, and J. P. Kutter, "Recent advances in lab-on-a-chip for biosensing applications," *Biosens. Bioelectron.*, vol. 76, pp. 213–233, 2016.

[6]   C. March *et al.*, "High-frequency phase shift measurement greatly enhances the sensitivity of QCM immunosensors," *Biosens. Bioelectron.*, vol. 65, pp. 1–8, Mar. 2015.

[7]   L. Cervera-Chiner *et al.*, "High Fundamental Frequency Quartz Crystal Microbalance (HFF-QCM) immunosensor for pesticide detection in honey," *Food Control*, vol. 92, pp. 1–6, Oct. 2018.

[8]   L. Cervera-Chiner, C. March, A. Arnau, Y. Jiménez, and Á. Montoya, "Detection of DDT and carbaryl pesticides in honey by means of immunosensors based on high fundamental frequency quartz crystal microbalance (HFF-QCM)," *J. Sci. Food Agric.*, vol. 100, no. 6, pp. 2468–2472, Apr. 2020.

[9]   L. Cervera-Chiner *et al.*, "High Fundamental Frequency Quartz Crystal Microbalance (HFF-QCMD) Immunosensor for detection of sulfathiazole in honey," *Food Control*, vol. 115, no. september, p. 107296, Sep. 2020.

[10]   G. Sauerbrey, "Verwendung von Schwingquarzen zur Wägung dünner Schichten

und zur Mikrowägung," *Zeitschrift für Phys.*, vol. 155, no. 2, pp. 206–222, 1959.

[11] R. Fernández, P. García, M. García, J. García, Y. Jiménez, and A. Arnau, "Design and Validation of a 150 MHz HFFQCM Sensor for Bio-Sensing Applications," *Sensors*, vol. 17, no. 9, p. 2057, Sep. 2017.

[12] P. Kao, D. Allara, and S. Tadigadapa, "Fabrication and performance characteristics of high-frequency micromachined bulk acoustic wave quartz resonator arrays," *Meas. Sci. Technol.*, vol. 20, no. 12, p. 124007, Dec. 2009.

[13] T. Tatsuma, Y. Watanabe, N. Oyama, K. Kitakizaki, and M. Haba, "Multichannel quartz crystal microbalance," *Anal. Chem.*, vol. 71, no. 17, pp. 3632–3636, 1999.

[14] W. Tao, P. Lin, Y. Ai, H. Wang, S. Ke, and X. Zeng, "Multichannel quartz crystal microbalance array: Fabrication, evaluation, application in biomarker detection," *Anal. Biochem.*, vol. 494, pp. 85–92, Feb. 2016.

[15] J. Rabe, S. Büttgenbach, J. Schröder, and P. Hauptmann, "Monolithic miniaturized quartz microbalance array and its application to chemical sensor systems for liquids," *IEEE Sens. J.*, vol. 3, no. 4, pp. 361–368, 2003.

[16] J. R. Vig, R. L. Filler, and Y. Kim, "Uncooled IR imaging array based on quartz microresonators," *J. Microelectromechanical Syst.*, vol. 5, no. 2, pp. 131–137, 1996.

[17] T. Abe and M. Esashi, "One-chip multuchannel quartz crystal microbalance fabricated by deep RIE," *Sensors Actuators A Phys.*, vol. 82, pp. 139–143, 2000.

[18] V. N. Hung, T. Abe, P. N. Minh, and M. Esashi, "Miniaturized, highly sensitive single-chip multichannel quartz-crystal microbalance," *Appl. Phys. Lett.*, vol. 81, no. 26, pp. 5069–5071, 2002.

[19] A. Tuantranont, A. Wisitsora-at, P. Sritongkham, and K. Jaruwongrungsee, "A review of monolithic multichannel quartz crystal microbalance: A review," *Anal. Chim. Acta*, vol. 687, no. 2, pp. 114–128, 2011.

[20] R. Fernandez *et al.*, "High Fundamental Frequency (HFF) Monolithic Resonator Arrays for Biosensing Applications: Design, Simulations, Experimental Characterization," *IEEE Sens. J.*, vol. Accepted, pp. 1–1, 2020.

[21] G. A. McCubbin *et al.*, "QCM-D fingerprinting of membrane-active peptides," *Eur. Biophys. J.*, vol. 40, no. 4, pp. 437–446, 2011.

[22] D. Johannsmann, *The Quartz Crystal Microbalance in Soft Matter Research*. Cham: Springer International Publishing, 2015.

[23] R. Lucklum, D. Soares, and K. Kanazawa, "Models for resonant sensors," in *Piezoelectric Transducers and Applications*, Second Edi., A. Arnau, Ed. Springer Berlin Heidelberg, 2008, pp. 63–96.

[24] J. Petri, S. Hochstädt, T. Nentwig, A. Pausch, A. Langhoff, and D. Johannsmann, "A Fast Electrochemical Quartz Crystal Microbalance,which Acquires Frequency and Bandwidth on Multiple Overtones," *Electroanalysis*, vol. 29, no. 3, pp. 806–813, Mar. 2017.

[25] M. Ferrari, V. Ferrari, and D. Marioli, "Interface circuit for multiple-harmonic analysis on quartz resonator sensors to investigate on liquid solution

microdroplets," *Sensors Actuators, B Chem.*, vol. 146, no. 2, pp. 489–494, 2010.

[26] H. Ogi, H. Naga, Y. Fukunishi, M. Hirao, and M. Nishiyama, "170-MHz Electrodeless Quartz Crystal Microbalance Biosensor: Capability and Limitation of Higher Frequency Measurement," *Anal. Chem.*, vol. 81, no. 19, pp. 8068–8073, Oct. 2009.

[27] Y. Montagut, J. V. García, Y. Jiménez, C. March, Á. Montoya, and A. Arnau, "Validation of a Phase-Mass Characterization Concept and Interface for Acoustic Biosensors," *Sensors*, vol. 11, no. 5, pp. 4702–4720, Apr. 2011.

[28] A. Arnau, "A Review of Interface Electronic Systems for AT-cut Quartz Crystal Microbalance Applications in Liquids," *Sensors*, vol. 8, no. 1, pp. 370–411, Jan. 2008.

[29] E. Uttenthaler, M. Schräml, J. Mandel, and S. Drost, "Ultrasensitive quartz crystal microbalance sensors for detection of M13-Phages in liquids," *Biosens. Bioelectron.*, vol. 16, no. 9–12, pp. 735–743, 2001.

[30] B. Zimmermann, R. Lucklum, P. Hauptmann, J. Rabe, and S. Büttgenbach, "Electrical characterisation of high-frequency thickness-shear-mode resonators by impedance analysis," *Sensors Actuators B Chem.*, vol. 76, no. 1–3, pp. 47–57, Jun. 2001.

[31] A. Arnau, Y. Montagut, J. V García, and Y. Jiménez, "A different point of view on the sensitivity of quartz crystal microbalance sensors," *Meas. Sci. Technol.*, vol. 20, no. 12, p. 124004, Dec. 2009.

[32] Y. Montagut, J. Garcia, Y. Jimenez, C. March, A. Montoya, and A. Arnau, "QCM Technology in Biosensors," in *Biosensors - Emerging Materials and Applications*, InTech, 2011.

[33] Y. J. Montagut, J. V. García, Y. Jiménez, C. March, A. Montoya, and A. Arnau, "Frequency-shift vs phase-shift characterization of in-liquid quartz crystal microbalance applications," *Rev. Sci. Instrum.*, vol. 82, no. 6, p. 064702, Jun. 2011.

[34] A. Guha, N. Sandström, V. P. Ostanin, W. van der Wijngaart, D. Klenerman, and S. K. Ghosh, "Simple and ultrafast resonance frequency and dissipation shift measurements using a fixed frequency drive," *Sensors Actuators B Chem.*, vol. 281, pp. 960–970, Feb. 2019.

[35] A. Guha *et al.*, "Direct detection of small molecules using a nano-molecular imprinted polymer receptor and a quartz crystal resonator driven at a fixed frequency and amplitude," *Biosens. Bioelectron.*, vol. 158, no. January, 2020.

[36] D. S. Ralf Lucklum, Kay Kanazawa, *Piezoelectric Transducers and Applications*. Berlin, Heidelberg, Heidelberg: Springer Berlin Heidelberg, 2008.

[37] K. Kanazawa, S. M. Yoon, and N. J. Cho, "Analyzing spur-distorted impedance spectra for the QCM," *J. Sensors*, vol. 2009, pp. 1–8, 2009.

[38] R. Lucklum, C. Behling, R. W. Cernosek, and S. J. Martin, "Determination of complex shear modulus with thickness shear mode resonators," *J. Phys. D. Appl. Phys.*, vol. 30, no. 3, pp. 346–356, Feb. 1997.

[39] J. A. Nelder and R. Mead, "A Simplex Method for Function Minimization,"

Comput. J., vol. 7, no. 4, pp. 308–313, Jan. 1965.

[40] M. L. sheely, "Glycerol Viscosity Tables," *Ind. Eng. Chem.*, vol. 24, no. 9, pp. 1060–1064, Sep. 1932.

[41] K. K. Kanazawa and J. G. Gordon, "Frequency of a quartz microbalance in contact with liquid," *Anal. Chem.*, vol. 57, no. 8, pp. 1770–1771, Jul. 1985.

[42] R. Fernández *et al.*, "High Fundamental Frequency (HFF) Monolithic Resonator Arrays for Biosensing Applications: Design, Simulations, Experimental Characterization," *IEEE Sens. J.*, vol. Accepted, 2020.

[43] A. Tsortos, G. Papadakis, and E. Gizeli, "Acoustic wave biosensor for detecting DNA conformation; A study with QCM-D," in *2008 IEEE International Frequency Control Symposium*, 2008, vol. 24, no. 4, pp. 346–349.

[44] A. Tsortos, G. Papadakis, and E. Gizeli, "Shear acoustic wave biosensor for detecting DNA intrinsic viscosity and conformation: A study with QCM-D," *Biosens. Bioelectron.*, vol. 24, no. 4, pp. 836–841, Dec. 2008.

[45] P. M. Wolny, J. P. Spatz, and R. P. Richter, "On the Adsorption Behavior of Biotin-Binding Proteins on Gold and Silica," *Langmuir*, vol. 26, no. 2, pp. 1029–1034, Jan. 2010.

[46] H. C. W. Hays, P. A. Millner, and M. I. Prodromidis, "Development of capacitance based immunosensors on mixed self-assembled monolayers," *Sensors Actuators B Chem.*, vol. 114, no. 2, pp. 1064–1070, Apr. 2006.

[47] S. Boujday, A. Bantegnie, E. Briand, P. G. Marnet, M. Salmain, and C. M. Pradier, "In-depth investigation of protein adsorption on gold surfaces: Correlating the structure and density to the efficiency of the sensing layer," *J. Phys. Chem. B*, vol. 112, no. 21, pp. 6708–6715, 2008.

[48] D. Johannsmann, I. Reviakine, and R. P. Richter, "Dissipation in films of adsorbed nanospheres studied by quartz crystal microbalance (QCM)," *Anal. Chem.*, vol. 81, no. 19, pp. 8167–8176, Oct. 2009.

Román Fernández is a Research and Development manager at AWSensors and an Associated Professor at Universitat Politècnica de València (UPV), Spain. He received his Ph.D. degree from UPV in 2003. His current research interests are focused on acoustic wave sensors for biosensing applications.

María Calero obtained her bachelor and master's degree from Universitat Politècnica de València in 2015 and 2017 respectively in telecommunication engineering. She is currently developing her PhD about acoustic array sensors in Universitat Politècnica de València.

Dr. José Vicente García-Narbón, chief technology officer (CTO) at AWSensors, received the Telecommunications Engineering (2007) and Ph.D. degrees (2016) from Universitat Politècnica de València (UPV), Spain. Since 2002, he has been working on the design of electronics interfaces for piezoelectric sensors, precision electronics, embedded systems, and acoustic wave sensors and its applications.

Dr. Ilya Reviakine is a chief application scientist at AWSensors and an Affiliate Professor at the University of Washington in Seattle. He specializes in biological surfaces and interfaces, interactions between biological systems (lipids, blood) and surfaces of artificial materials, and surface acoustic sensing. Previously, he led independent research groups in Spain and in Germany. As a recipient of the prestigious Alexander von Humboldt research fellowship, he worked on hydrodynamic effects in surface-acoustic sensing. His doctoral work on atomic force microscopy of biological macromolecules and their assemblies earned him a Paper of the Year award from the Journal of Structural Biology.

Antonio Arnau received the Engineering and Ph.D. degrees from Universitat Politècnica de València (UPV), Spain, in 1990 and 1999, respectively. Since 1990 he has been working on the design of electronics and communication electronics circuits and acoustic wave sensors. His current research interests include piezoelectric transducers and applications. He is author of more than 50 international papers and books; he has 5 patents and has taught classes and seminars in over 25 foreign institutions. He has created two spin-off companies: AWSensors focused on acoustic sensors and its

applications to biotechnology and AWSensors Diagnostics, focused on Point of Care, Point of Diagnostics and Mobile Health Applications market.

Yolanda Jimenez received the degree of Telecommunications Engineer and the PhD from Universitat Politècnica de València in 1999 and 2004, respectively. She had obtained more than 30 research publications and is co-author of 2 patents, both internationally extended and in operation by the Spin-off company UPV AWSensors, of which she is a founding partner. Since she joined to the staff of UPV in 2000, her research has been focused on acoustic wave sensors, particularly in piezoelectric resonators, including their modelling, applications with biosensors, design of characterization systems and development of mathematical algorithms for the extraction of the physical parameters of the sensor